

## Effects of biomass burning in Amazonia on climate: A numerical experiment with a statistical-dynamical model

Elisabete C. Moraes

Divisão de Sensoriamento Remoto, Instituto Nacional de Pesquisas Espaciais (INPE), São José dos Campos, SP, Brazil

Sergio H. Franchito and V. Brahmananda Rao

Centro de Previsão de Tempo e Estudos Climáticos, Instituto Nacional de Pesquisas Espaciais (INPE), São José dos Campos, SP, Brazil

Received 23 May 2003; revised 2 December 2003; accepted 11 December 2003; published 13 March 2004.

[1] Chou and Suarez's solar and infrared radiation models are incorporated in a statistical-dynamical model with biosphere and atmosphere interaction in order to study the climatic effects due to biomass burning in Amazonian forest. In the control experiment the mean annual zonally averaged climate is well simulated by the model when compared with observed data. Biomass burning plays an important role on the earth's radiative balance and climate through the release of large amounts of greenhouse gases and aerosols in the atmosphere and the alteration of the land surface characteristics. For investigating the relative importance of these changes five experiments are performed: (1) degradation of the surface, (2) change in the smoke aerosols concentration, (3) change in the CO<sub>2</sub> concentration, (4) change in CH<sub>4</sub> concentration, and (5) all the changes together. The results show that biomass burning in Amazonian forest causes a reduction in the absorbed solar radiation and net radiation fluxes at the surface in the perturbed region and an increase in the air surface temperature and the net thermal infrared radiation flux at the surface. Also there is a decrease in the latent and sensible heat fluxes, evapotranspiration and precipitation compared to the control case. In general, the greater changes in the radiative balance and climate are due mainly to the changes in the land surface characteristics, followed by those caused by the large amounts of smoke aerosols released in the atmosphere. The changes due to the greenhouse gases CO<sub>2</sub> and CH<sub>4</sub> are small.

*INDEX TERMS:* 3359 Meteorology and Atmospheric Dynamics: Radiative processes; 0305 Atmospheric Composition and Structure: Aerosols and particles (0345, 4801); 0315 Atmospheric Composition and Structure: Biosphere/atmosphere interactions; 0360 Atmospheric Composition and Structure: Transmission and scattering of radiation; *KEYWORDS:* biomass burning, radiative balance, biosphere and atmosphere interaction

**Citation:** Moraes, E. C., S. H. Franchito, and V. Brahmananda Rao (2004), Effects of biomass burning in Amazonia on climate: A numerical experiment with a statistical-dynamical model, *J. Geophys. Res.*, 109, D05109, doi:10.1029/2003JD003800.

### 1. Introduction

[2] Widely prevalent in the tropics, anthropogenic biomass burning expanded drastically in the last decades due to the increased deforestation practices in the Brazil's Amazon basin as well as to clear land for shifting cultivation in South America, Southeast Asia and Africa (<http://www.gvm.jrc.it/fire/gba200/index.html>). Biomass burning is considered to be one of the major sources of greenhouse gases and tropospheric aerosols [Crutzen *et al.*, 1979]. Aerosols can modify the radiation balance by an increase of solar radiation reflection, thus reducing the energy gain of the earth-atmosphere system, by an increase of solar absorption in the atmosphere and by a change of the upward thermal infrared radiation through increased longwave opacity. The

relative importance of these effects, resulting in a cooling or a warming of the atmosphere, depends on the absorption and scattering properties of the aerosols. Many studies have been devoted to examine the effects of smoke aerosols on the radiative balance in the Amazonian region [Christopher *et al.*, 1998; Tarasova *et al.*, 2000, 1999]. Greenhouse gases have high transmissivity to solar radiation and high absorptivity to longwave radiation. This implies a smaller planetary outgoing longwave radiation flux to space and, consequently, warming of the climate system. Studies about the release of greenhouse gases in the Amazonian region were made by Alvalá *et al.* [1996] and Babbitt *et al.* [1996].

[3] In addition to its influence on the radiation budget biomass burning in Amazonia also modifies the land surface characteristics. This implies a decrease of evapotranspiration and precipitation associated with altered general circulation patterns [Nobre *et al.*, 1991]. Although several studies have examined the impacts of biomass burning in Amazonia

on the radiative balance and climate, the relative importance of the changes and mechanisms involved have not been investigated. Are all the changes of the same magnitude or is there a main mechanism responsible for the change? The objective of the present paper is to study the relative contributions of the changes in the radiation budget and climate caused by smoke aerosols, greenhouse gases and alteration of the land surface characteristics due to biomass burning in the Amazonian forest. For this purpose, a coupled biosphere-atmosphere statistical-dynamical model (SDM) with a detailed parameterization of the radiative processes is used. This kind of model is essentially mechanistic, being directed toward understanding the dependence of a particular mechanism on the other parameters of the problem.

[4] In section 2 the biosphere-atmosphere coupled SDM and the radiation model are presented. The model validation is shown in section 3. In section 4 the biomass burning experiment is presented, and section 5 contains the summary and conclusions.

## 2. The Model

[5] The SDM used in this study is a coupled biosphere-atmosphere climate model developed by *Varejão-Silva et al.* [1998] (hereafter called VS). In the present work the simple formulations of the radiative fluxes in VS are improved taking into account the effects of the main absorbing and emitting gases in the atmosphere. For this purpose, the original formulations of the radiative fluxes used by VS are replaced by a detailed radiation model developed by *Chou and Suarez* [1994, 1999]. This will permit a detailed study of the radiative effects of greenhouse gases emitted during biomass burning on climate.

### 2.1. Description of the SDM

[6] The SDM is a two-layer zonally averaged global primitive equation model that uses a sigma vertical coordinate and horizontal resolution of  $10^\circ$  latitude. The SDM includes parameterizations of friction, diabatic heating and large-scale eddies. The energy fluxes such as solar radiation, thermal infrared radiation, sensible and latent heat fluxes, and subsurface flux are computed separately for the land fraction and the remaining part (covered by ocean-ice-snow) of the latitude belt. The parameterizations of the biosphere model based on BATS (Biosphere-Atmosphere Transfer Scheme) [Zhang, 1994] are used for the land fraction of the latitude belt. For the fraction of the earth's surface covered by ocean, ice and snow parameterizations similar to those from the biosphere model are used, but only the effects of ocean-ice-snow are considered.

[7] The parameterizations of the components of the surface and atmospheric fluxes for the fraction of the earth's surface covered by land (soil and vegetation) are given in Tables 1–3 of VS and the formulations for the surface and atmospheric fluxes for the remaining portion of a latitude belt (ocean-ice-snow) are given in Table 5 of VS. The values of the components of surface and atmospheric fluxes for a latitude belt as a whole are obtained through the weighted-mean of these values for the fractions of the earth's surface covered by land and by ocean-ice-snow, using as weight the portions of land and ocean-ice-snow

in a latitude belt. More details about the coupled biosphere-atmosphere SDM are given in VS.

### 2.2. The Radiation Model

[8] The thermal infrared (or longwave) and solar radiation parameterization schemes used in this work are those developed by *Chou and Suarez* [1994] and *Chou and Suarez* [1999], respectively. *Chou and Suarez's* [1994] original model assumes a blackbody infrared emissivity. In a more recent version of the model, they consider the surface emissivity in 10 spectral bands (M.-D. Chou, personal communication, 2000). In the present study, the new version of the model is used. These schemes use several broadband parameterization schemes for thermal infrared and solar radiation to produce a computationally fast and accurate representation of radiation processes. The original version of the radiation model considers the entire atmosphere divided into 75 layers. In order to couple the radiation code to the SDM 20 layers are used. Details about the coupling of the models are given in section 2.3.

[9] The solar radiation parameterization includes the absorption due to ozone, water vapor, oxygen, carbon dioxide, cloud and aerosols and multiple-scattering due to clouds, aerosols and gases. Rayleigh scattering and cloud reflection are treated using a two-stream method for a range of conditions varying from cloudy sky of arbitrary optical depth to clear sky. The ultraviolet (UV) and visible region is grouped into 8 bands (7 in the UV region and 1 in the photosynthetically active radiation, PAR). An effective coefficient for ozone absorption and an effective cross section for Rayleigh scattering are computed for each band. In the near infrared region, the broadband parameterization is used to compute the absorption by water vapor in a clear atmosphere. This region is grouped into 3 bands which are divided into 10 subbands. The k-distribution method is applied to calculate fluxes in a scattering atmosphere. The reflectivity and transmissivity of a scattering atmosphere are computed using the delta-four-stream approximation.

[10] For longwave absorption, broadband transmission functions of water vapor [Chou, 1984], carbon dioxide [Chou and Peng, 1983] and ozone [Chou and Kouvaris, 1986] are used. The approach relies on parameterizations of diffusive transmittance functions appropriately weighted by the Planck blackbody source terms. The scheme includes the water vapor line and continuum absorption, carbon dioxide absorption through band centers and band wing regions, and infrared ozone-absorption bands. The infrared radiative transfer model also computes the fluxes due to trace gases ( $\text{N}_2\text{O}$ ,  $\text{CH}_4$ ,  $\text{CFC}_{11}$ ,  $\text{CFC}_{12}$ ,  $\text{CFC}_{22}$ ,  $\text{CO}_2$ -minor), clouds and aerosols.

[11] Detailed descriptions of the radiation models are given by *Chou and Suarez* [1994, 1999].

### 2.3. Inclusion of the Radiation Models in the SDM

[12] In order to incorporate the thermal infrared and solar radiation models in the SDM the original formulation of these fluxes in VS are replaced by those given by *Chou and Suarez* [1994, 1999]. For this purpose, the solar radiation and infrared models are applied separately for each type of surface in a latitude belt: soil, vegetation and the portion with ocean-ice-snow.

[13] Chou and Suarez radiation models contain 75 atmospheric layers from the surface to 0.0001 hPa. Tests show that there was not significant modification in the simulation of zonally averaged solar and infrared radiation fluxes when the radiation models are run with either 75 or 20 layers. The differences in the simulation of the solar and thermal infrared radiation fluxes are less than 2%. In the present work, only 20 atmospheric layers are used in order to reduce computational time. The radiative fluxes are computed at each layer assuming that the entire atmospheric column is divided into 20 layers. Since the SDM is a two-layer model (one layer from 1000 hPa to 500 hPa, and the other from 500 hPa to the top of the atmosphere (TOA)) the total amount of solar and thermal infrared radiation absorbed in the entire atmosphere is equally partitioned into the two SDM atmospheric layers. The net radiation heating in each model layer is required for the thermodynamic tendency equation calculation and, consequently, for computing the zonally averaged temperatures at 250 hPa and 750 hPa. Also, the net radiation heating at the surface is needed for the calculation of the soil and foliage temperatures and the surface temperature at the portion of the latitude belt covered by ocean-ice-snow. The SDM, in turn, provides the values of the surface temperatures which are necessary for computing the radiative fluxes in these portions of the latitude belt.

[14] Although the SDM is a two-layer model, the results discussed later show that it is capable of simulating the observed zonally averaged climate and provide useful results of sensitivity experiments. As mentioned earlier in the introduction, the model used in this study is a mechanistic model with minimum resolution yet capable of incorporating detailed radiation parameterizations.

#### 2.4. Input Data for Running the Radiation Models

[15] The input data for the radiation models are the mean annual zonally averaged values of the vertical profiles of temperature, specific humidity and ozone mixing-ratios, cloud and aerosol optical properties, the spectral surface emissivity, the direct and diffuse spectral reflectance in the region of UV and PAR ( $\lambda \leq 0.7 \mu\text{m}$ ) and in the near infrared region ( $\lambda > 0.7 \mu\text{m}$ ), and the mixing-ratio of the absorbing gases.

[16] The vertical profiles of temperature, specific humidity and ozone mixing-ratios needed to run the radiation models are obtained from Chou [2000]. They are based on the optical properties of the atmosphere defined by McClatchey *et al.* [1972] and correspond to the mean annual values for the standard atmosphere in tropical, middle and high latitudes. These values are used above 750 hPa in all the cases of the radiation models applying to the regions of soil, vegetation and ocean-ice-snow. However, the vertical profiles of temperature and specific humidity at low levels (between the surface and 750 hPa) depend strongly on the values of these variables at the surface. Therefore they are modified at each time step according to the surface temperatures at soil, vegetation and ocean-ice-snow. The vertical profile of temperature is obtained assuming a moist adiabatic lapse rate and the values of the specific humidity at low levels are obtained from the empirical expression given by Franchito *et al.* [1998].

[17] The cloud amount in each latitude belt is provided by the SDM. The specification of clouds in the latitude belt is made according the following procedure. The type of clouds (high, middle and low) is defined considering the pressure levels given by Chou and Suarez [1999], i.e., 400 hPa and 700 hPa. In order to determine the type of clouds and cloud layer thickness in the latitude belt the values of the height of top and bottom of clouds given by Peixoto and Oort [1992] are used. These values are compared to the height of the 400 and 700 hPa pressure levels for obtaining the type of clouds. The difference between the top height and base height implies in the cloud layer thickness. The cloud optical thickness in each latitude belt is obtained from the climatological values given by Hahn *et al.* [2001].

[18] The data of aerosols optical thickness and single-scattering albedo are obtained from the mean annual values simulated by the SI99 model (GISS/NASA) for 1999 (<http://www.giss.nasa.gov/data/model/>). Taking into account that the larger concentration of aerosols occurs in the layers lower than 800 hPa it is considered in the SDM that the aerosols are present only below 800 hPa. Since the radiation models need the vertical profile of the aerosols optical thickness it is assumed that the mean annual zonally averaged aerosols optical thickness in each layer is given by the ratio between the total aerosols optical thickness and the number of layers from the surface to 800 hPa. The mean annual zonally averaged asymmetry factor is given by the average of the typical values of continental and ocean aerosols given by the *World Meteorological Organization* [1986].

[19] The values of the spectral reflectance in the region of UV and PAR ( $\lambda \leq 0.7 \mu\text{m}$ ) and in the near infrared region ( $\lambda > 0.7 \mu\text{m}$ ) for each type of surface are given by BATS [Dickinson *et al.*, 1986]. However, in the present work for  $\lambda > 0.7 \mu\text{m}$  the spectral reflectance of water bodies (ocean and inland water) is modified because the water bodies absorb almost all the solar irradiance in these wavelengths. Since the spectral reflectance is proportional to the ratio between the backscattering coefficient and the absorption coefficient, for the near infrared region its value is close to zero [Mobley, 1994]. So, the values are changed from 0.2 (given by BATS) to 0.01 (present model). The spectral emissivities of each type of vegetation according to BATS are the same as those given by Wilber *et al.* [1999] which were obtained from a radiative transfer model [Fu and Liou, 1992]. The concentration of the greenhouse gases used in the radiation models is obtained from Houghton *et al.* [2001], i.e., 360 ppm and 1.76 ppm for  $\text{CO}_2$  and  $\text{CH}_4$ , respectively.

#### 2.5. Initial Conditions

[20] The SDM has  $10^\circ$  latitude resolution and employs a latitudinal centered finite-differencing scheme. The strategy for running the SDM is similar to that used by VS. First, the SDM without the inclusion of the biosphere parameterization is integrated using as initial condition an isothermal atmosphere (270 K) at rest. An explicit time integration was used with a time step of 30 minutes. The SDM is integrated for a six month period forced by mean annual conditions in order to obtain stationary solutions. In a second step, the SDM is run for a six month period including the effects of the biosphere. Since the values of the 500 hPa temperature and the wind speed are necessary to run the biosphere-

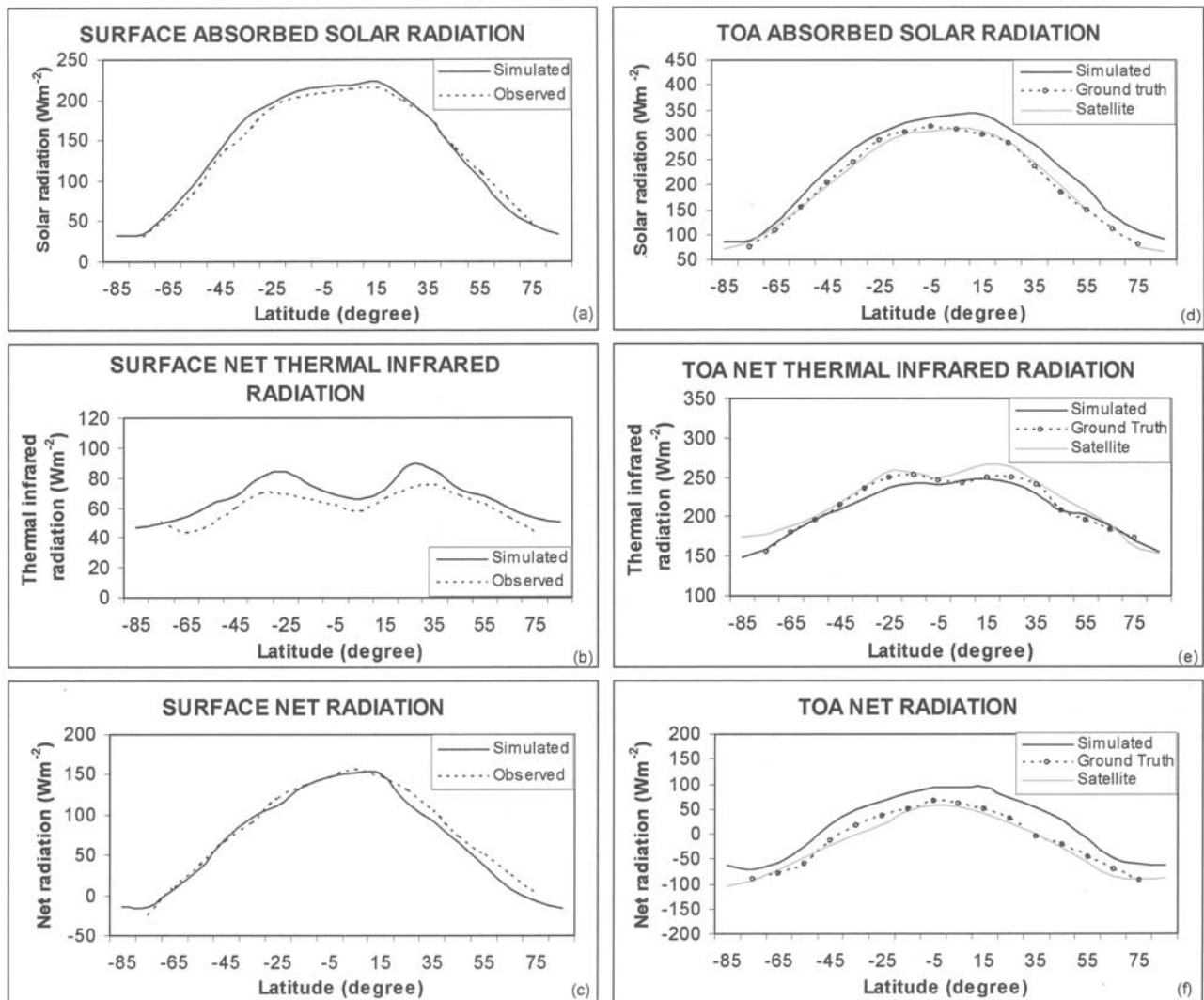


**Figure 1.** Simulated and observed mean annual values of the surface and planetary fluxes: absorbed solar radiation (a) and (d), net thermal infrared radiation (b) and (e), and net radiation (c) and (f). The model values correspond to the thick solid line. Ground truth data [Ou *et al.*, 1989] are represented by dashed line (Figures 1a–1c); in Figures 1d–1f ground truth data [Campbell and Vonder Haar, 1980] and satellite data [Ellis and Vonder Haar, 1976] are represented by the short-dashed line with open circles and by thin solid line, respectively. Units,  $W m^{-2}$ .

atmosphere coupled SDM they cannot be zero in the initial conditions. So, the mean annual zonally averaged simulation obtained earlier is used as an initial condition for running the coupled biosphere-atmosphere model. Comparing to VS, the main difference in the strategy of running the coupled biosphere-atmosphere SDM consists in the fact that in the present study in the second step of the integration the radiation models [Chou and Suarez, 1994, 1999] are applied separately to the regions of soil, vegetation and ocean-ice-snow, as mentioned in section 2.3.

### 3. Model Validation

[21] The coupled biosphere-atmosphere SDM is run using mean annual conditions in order to simulate the zonally averaged climate. First, the simulation of the radiative fluxes is shown. In the second part the simulation of the

SDM variables (temperature, zonal winds, precipitation, etc) is presented.

#### 3.1. Radiation Quantities

[22] In this section some of the radiation quantities simulated by the model are compared with observed data for mean annual conditions. Figures 1a–1c show the simulated and observed absorbed solar radiation, net thermal infrared radiation and net radiation fluxes at the surface. Observed data are obtained from Ou *et al.* [1989]. As can be seen, there is a good agreement between the model results and the observations although the simulated values are somewhat overestimated compared to the observations in the case of the net thermal infrared radiation.

[23] Figures 1d–1f show the latitudinal variation of the planetary values of the absorbed solar radiation, net thermal infrared and net radiation fluxes. Also shown

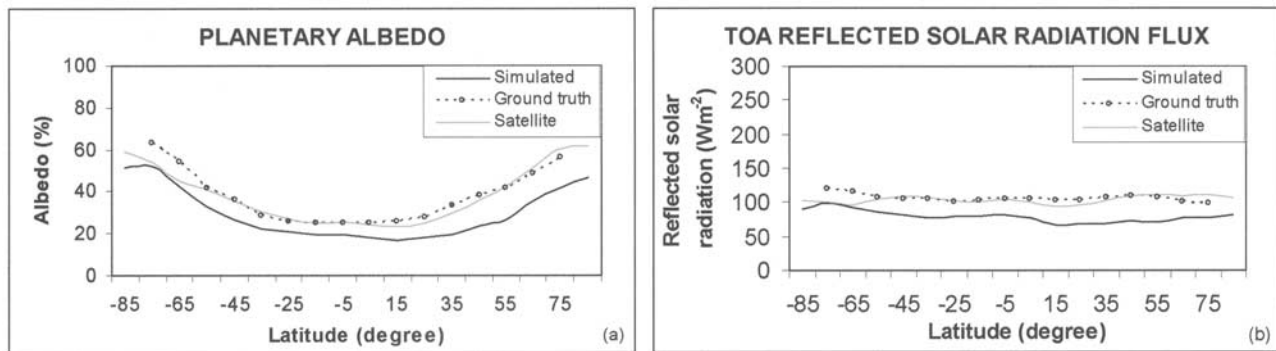


**Figure 2.** Simulated and observed mean annual: (a) planetary albedo, and (b) reflected solar radiation flux at the top of the atmosphere ( $\text{W m}^{-2}$ ). The model values correspond to the thick solid line and ground truth data [Campbell and Vonder Haar, 1980] and satellite data [Ellis and Vonder Haar, 1976] are represented by the short-dashed line with open circles and by thin solid line, respectively.

are the ground truth data from Campbell and Vonder Haar [1980] and satellite data [Ellis and Vonder Haar, 1976]. As can be seen in Figures 1d and 1f, the simulated values of the absorbed solar radiation and net radiation fluxes agree reasonably well with the observations. However, the model values are slightly overestimated compared to the observations, mainly in the Northern Hemisphere. This is due to the underestimation of the modelled planetary albedo, as can be noted in Figure 2a. As shown in Figure 1e, there is a good agreement between the simulated and observed net thermal infrared radiation. The simulation is closer to the observations when the model values are compared with the data from Campbell and Vonder Haar [1980]. The simulated values are in general a little underestimated when compared to the satellite observations.

[24] Figure 2a show that there is a reasonably good agreement between the simulated and observed mean annual planetary albedo although the model values are in general underestimated. Consequently, the reflected solar radiation flux at the top of the atmosphere is underestimated (Figure 2b). It should be mentioned that the satellite observations correspond to the period from 1964 to 1971 and contain uncertainties which vary from 8% in the polar region to 10% in the equatorial region [Ellis and Vonder Haar, 1976].

[25] In order to verify the statistical significance of the results we calculated the correlation coefficient (c.c) between the modelled values and the ground truth data [Campbell and Vonder Haar, 1980]. We use the two

sided Student t-test to verify the significance of the correlations. The c.c are calculated for the latitudinal region between 75°S to 75°N, where the observed data are available. The results show that the c.c between the simulated and observed values of the surface and planetary fluxes of absorbed solar radiation, net infrared thermal infrared radiation and net radiation are higher than 0.94, significant at the 99% confidence level.

[26] Next, the mean annual global values of radiative quantities simulated by the model are compared with observed data and GCM simulations. Table 1 shows the simulated and observed mean annual global values of the planetary albedo, reflected solar radiation flux at the top of the atmosphere, solar radiation fluxes absorbed at the surface and by the atmosphere. Also shown are the comparisons with two data sources: ERBE/Ohmura, which corresponds to observations from the world net of pyranometers [Ohmura and Gilgen, 1991] in addition to satellite data from ERBE [Barkstrom et al., 1989], and ERBE/Li, which corresponds to observations from satellite data (ERBE), where the surface solar radiation fluxes are estimated using the Li and Leighton [1993] algorithm. As can be noted, there is a good agreement between the simulated planetary albedo and the observed values from the two data sources. The value of the solar radiation flux absorbed by the atmosphere simulated by the model is contained in the range of the observed values. The simulated value of the solar radiation flux absorbed at the surface is closer to the observed value derived from observations in addition to satellite information (ERBE/

**Table 1.** Comparison Between Modeled Radiative Quantities and Observed Data<sup>a</sup>

Sources	Solar Radiation Flux Absorbed at the Surface	Solar Radiation Flux Absorbed by the Atmosphere	Solar Radiation Flux Reflected at the Top of the Atmosphere	Planetary Albedo
present SDM	132.0	88.7	79.3	29.6
ERBE/Ohmura	142.0	98.0	101.3	29.6
ERBE/Li	157.0	83.1	101.3	29.6

<sup>a</sup>ERBE/Ohmura correspond to observations from the world net of pyranometers [Ohmura and Gilgen, 1991] in addition to satellite data from ERBE [Barkstrom et al., 1989]; ERBE/Li correspond to observations from satellite data (ERBE), where the surface solar radiation fluxes are estimated using the Li and Leighton [1993] algorithm. Units,  $\text{W m}^{-2}$ .

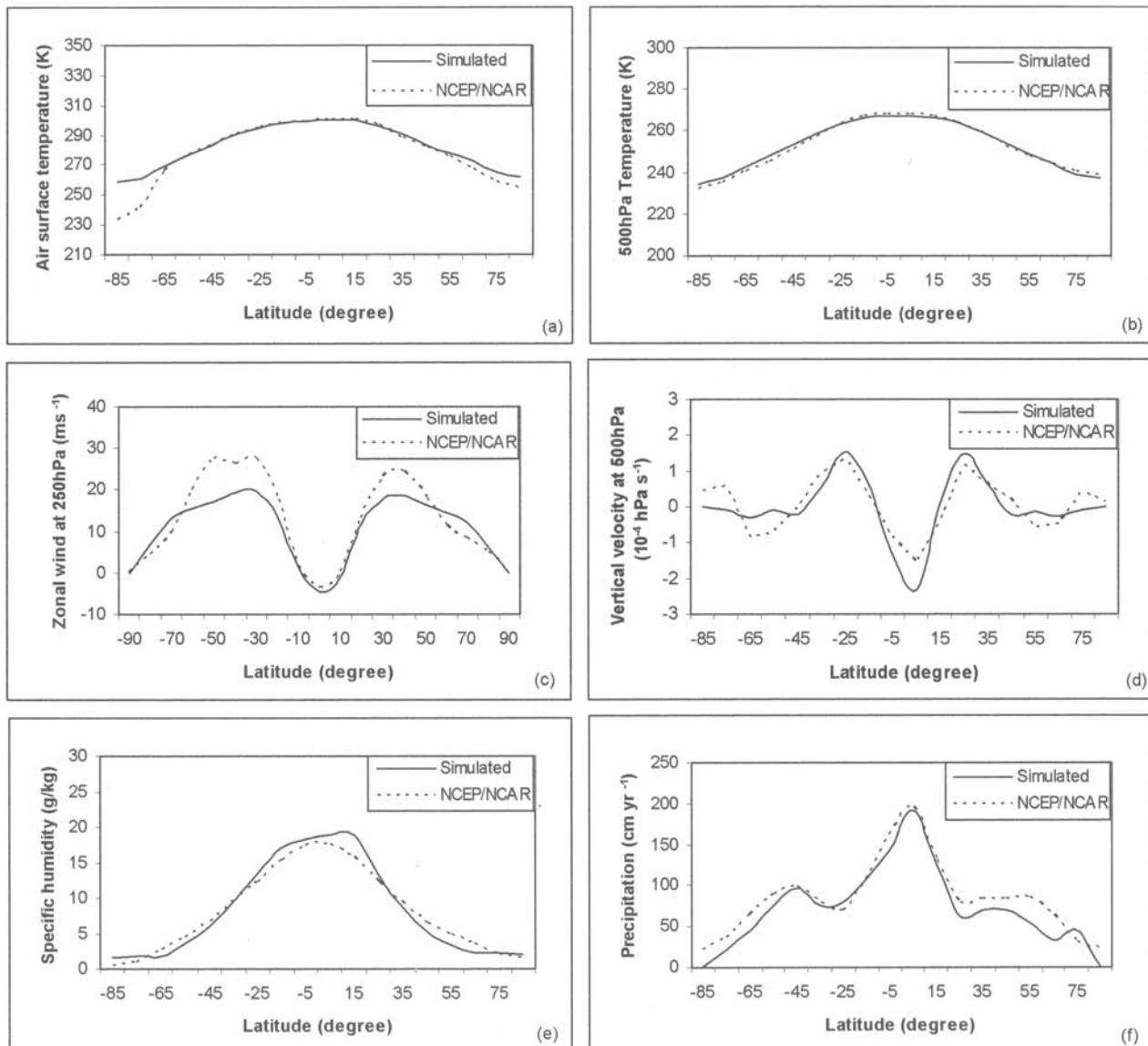


**Figure 3.** Simulated and observed zonally averaged characteristics: (a) air surface temperature (K), (b) 500 hPa temperature (K), (c) zonal wind at 250 hPa ( $\text{m s}^{-1}$ ), (d) vertical velocity at 500 hPa ( $10^{-4}$  hPa  $\text{s}^{-1}$ ), (e) specific humidity at the surface ( $\text{g/kg}$ ), and (f) precipitation ( $\text{cm yr}^{-1}$ ). The model values correspond to the thick solid line and the reanalysis data are represented by the short-dashed line.

Ohmura) while the modelled value of the reflected solar radiation flux at the top of the atmosphere is lower than the observed values. This may be related to the cloud physical properties considered in the model.

[27] Now, the SDM values of the mean annual global percentage of the surface and planetary net thermal radiation fluxes, thermal radiation downward onto surface and the solar radiation flux absorbed at the surface relative to the solar irradiance at the top of the atmosphere are compared to the best GCM estimates of these radiative quantities given by *Wild et al.* [1998]. Compared to the best GCM calculations the SDM results underestimate the surface absorbed solar radiation, the thermal radiation downward onto surface and the net thermal radiation emitted by planet by less than 3% and overestimate the surface net thermal radiation by less than

3.45%. Thus the partition of the radiative energy is very well simulated by the SDM.

### 3.2. Simulation of the Zonally Averaged Characteristics

[28] Figures 3a–3f show the simulated and observed zonally averaged air surface temperature, 500 hPa temperature, zonal wind at 250 hPa, vertical velocity at 500 hPa, specific humidity at the surface, and precipitation, respectively. The observed data are obtained from the National Centers for Environmental Prediction (NCEP)/National Center for Atmospheric Research (NCAR) reanalysis data sets. As can be seen in Figure 3, the agreement between the model simulations and the reanalysis data is good. The air surface and 500 hPa temperatures are well simulated by the model (Figures 3a–3b). The larger differences occur near

the polar regions, mainly in the Southern Hemisphere. Processes like the ice/snow albedo feedback seem to play an important role in these regions and should be included in the SDM in future in order to improve the model simulations. Since the deviations are in the same direction, the vertical temperature gradient (surface–500 hPa) is well simulated. The simulated values of the zonal wind at 250 hPa agree with those from the reanalysis data, although the magnitude of the jets is somewhat underestimated, mainly in the Southern Hemisphere (Figure 3c). It can be noted that the position of the jets and the easterlies in the tropical region are well simulated by the model. The three cells of mean meridional circulation can be seen in Figure 3d. The ascending motion in the tropical region and the subsidence in the subtropics and temperate latitudes are well simulated by the model, although the maximum ascending motion in the equatorial region is somewhat overestimated. The latitudinal variations of the specific humidity and the precipitation are in good agreement with the observed data (Figures 3e–3f). As can be seen in Figure 3f, maximum of the precipitation near the equator and the values in the tropical and subtropical regions are successfully well simulated by the model. The secondary maxima are also well reproduced, although the maximum is shifted equatorward in the Northern Hemisphere.

[29] The results presented above show that the mean annual zonally averaged radiative fluxes and climate characteristics are well simulated by the SDM. The simulation of the mean annual zonally averaged climate is taken as the control experiment in the next section.

#### 4. Simulation of the Climate Effects Due to Biomass Burning in Amazonia

[30] In this section the climatic effects due to biomass burning in Amazonia are investigated. Section 4.1 shows the description of the experiment and the results are presented in section 4.2.

##### 4.1. Description of the Experiment

[31] As mentioned earlier, the SDM takes into account the fraction of the Earth's surface covered by each type of vegetation according to BATS in each latitude belt. Consequently, the model allows us to investigate the climate change due to land surface modification in a determined region of a latitude belt, such as the Amazonian forest. In order to simulate the climatic effects of biomass burning in Amazonia the evergreen broadleaf trees are replaced by semi-desert in South America from 20°S to 10°N. So, all the characteristic parameters of the tropical forest are replaced by those of semi-desert conditions according to BATS, except the soil spectral reflectance. Since the dominant soil in the Amazonian region is the yellow oxisol (A. R. Formaggio, personal communication, 2001) the values of the soil spectral reflectance are changed to 0.1 (for  $\lambda < 0.7 \mu\text{m}$ ) and 0.35 (for  $\lambda > 0.7 \mu\text{m}$ ). The values of the variables used in the continental area of the latitude belt are obtained through the weighted-mean of the specific values using as weight the fraction of each type of vegetation in the latitude belt, but replacing the evergreen broadleaf trees by semi-desert. Although the SDM is designed to calculate zonal means and not exactly regional

features of Amazonian climate it allows us to obtain separately the simulations for the continental portion of a latitude belt. Since most of the continental area of the tropical region in South America is covered by Amazonian forest the effects of biomass burning in Amazonia climate are analysed taking into account the model simulations for the land fraction of the tropical region.

[32] The concentrations of CO<sub>2</sub> and CH<sub>4</sub> in the atmosphere are modified from 360 ppm and 1.76 ppm (control experiment) to 397.4 ppm and 1.9 ppm [Babbitt *et al.*, 1996], respectively, which are typical values after burning of tropical forest. Since the smoke gases and aerosols from fire events are transported over long distances, the modifications in their concentrations are considered over the entire latitude belts where the Amazonian forest is contained (20°S–10°N). In the other latitude belts the gases and aerosols concentrations are the same as those in the control experiment.

[33] The concentration of aerosol in the Amazonian region is higher during the drier period (June to September [Nobre *et al.*, 1998]) when the anthropogenic burning of forest occurs. However, in the present study it is assumed that the aerosols are present throughout the year. The aerosols optical thickness, single-scattering albedo and asymmetry factor are modified from 0.18, 0.9 and 0.85 (control experiment) to 0.336, 0.866 and, 0.623 respectively. These modifications are considered at  $\lambda = 0.5 \mu\text{m}$  (region of PAR). The mean annual value of the smoke aerosol optical thickness is obtained from the monthly mean values given by Holben *et al.* [2001]. These values correspond to AERONET (Aerosol Robotic Network) data for Alta Floresta (9.52°S, 56.0°W), which is a typical region of tropical rain forest with high anthropogenic influence. The values of the single-scattering albedo and the asymmetry factor of smoke aerosol are given by Tarasova *et al.* [1999]. Although these values are typical for the dry period in the present work they are assumed to represent mean annual conditions. It is supposed that the column aerosol optical depth extends from surface to 2 km and the aerosol concentration in each layer is constant. So, the mean annual aerosol optical thickness is divided by the number of model layers from the surface to 2 km.

[34] The climatic impact due to biomass burning in the Amazonian forest is studied considering separately the effects of the changes in the type of vegetation and in the greenhouse gases and aerosols concentrations. For this purpose, five experiments are carried out with the model: (1) changes in the aerosol concentration, (2) alterations in the CO<sub>2</sub> concentration, (3) alterations in the CH<sub>4</sub> concentration, (4) changes in all the surface parameters (tropical forest to semi-desert) and (5) all the changes simultaneously. As mentioned earlier, the simulation of the mean annual zonally averaged climate (sections 3.1–3.2) is taken as the control experiment.

##### 4.2. Results

[35] Figures 4a–4c show the changes in the radiative balance at the surface due to biomass burning in the Amazonian forest. Shown are the changes (perturbed minus control cases) in the continental areas of the latitude belts in the five experiments. As can be seen, the impact of smoke aerosols and gases is to reduce the

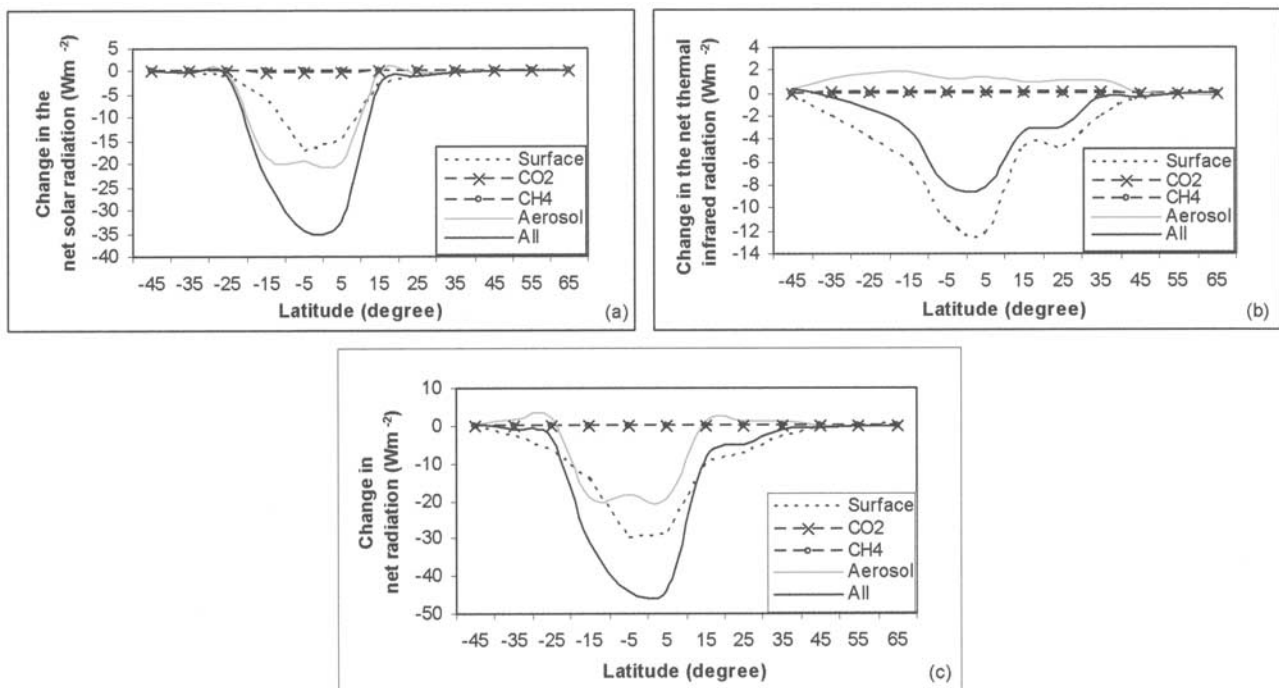


**Figure 4.** Changes in the absorbed solar radiation (a), net thermal infrared radiation (b), and net radiation (c) fluxes at the surface (perturbed minus control) in the continental portion of the latitude belt. Shown are the changes due to the aerosol concentration (thin solid line), CO<sub>2</sub> concentration (long-dashed line with x), CH<sub>4</sub> concentration (long-dashed line with open circles), land surface parameters (short-dashed line), and all the changes simultaneously (thick solid line). Units, W m<sup>-2</sup>.

absorbed solar radiation and the outgoing thermal infrared radiation at the surface. This is due to the increase of both the albedo of the atmosphere and the atmospheric opacity to longwave radiation, respectively. The changes due to gases effect are small. On an average over the continental areas of the latitude belts containing the Amazonian forest, smoke aerosols cause a decrease of 9.7% in the absorbed solar radiation and 2.2% in the outgoing thermal infrared radiation at the surface in relation to the mean annual value (Table 2). The direction of these changes is in agreement with those from observational [Christopher *et al.*, 1998] and radiation model studies [Tarasova *et al.*, 1999, 2000]. The changes due to the gases effect are less than 0.03% and 0.07% in the cases of net solar radiation and outgoing thermal infrared radiation, respectively. As can be noted the CH<sub>4</sub> effect is slightly smaller than that of CO<sub>2</sub>. The net radiation at the surface decreases in the aerosol experiment showing that the effect of the reduced absorbed solar radiation is greater than the effect of the outgoing longwave radiation decrease. This indicates that the effect of smoke aerosol on reflection, absorption and scattering of incoming solar radiation is greater than that from longwave opacity increase. The net radiation at the surface also decreases in the greenhouse gases experiment. However, the changes are smaller than those due to smoke aerosols. Smoke aerosols cause a decrease of 14.1% in the net radiation at the surface on an average over the continental areas of the latitude belts containing the Amazonian forest while the reduction due to CO<sub>2</sub> and CH<sub>4</sub> is less than 0.01%.

[36] Figures 4a–4c show that the effect of the degradation of the surface due to biomass burning in Amazonian forest on the radiative balance at the surface is similar to that obtained in most of deforestation numerical experiments using GCMs (Nobre *et al.* [1991], Dickinson and Kennedy [1992], Lean and Rowntree [1993, 1997], and many others). The absorbed solar radiation decreases due to the greater land surface albedo and the net infrared radiation increases due to higher surface temperature (Figure 6). Consequently, there is a decrease in the net radiation at the surface. On an average over the continental areas of the latitude belts comprising the Amazonian forest, the substitution of the tropical forest by semi-desert implies a decrease of 6.3% and 17.5% in relation to the annual mean absorbed solar radiation and net radiation at the surface, respectively, and an increase of 14.1% in the net thermal infrared radiation (Table 2). When the effects of smoke aerosols, CO<sub>2</sub> and CH<sub>4</sub> and degradation of the surface are taken into account together the absorbed solar radiation and net radiation at the surface are reduced by 15.3% and 29%, respectively, and the net infrared radiation is increased by 9.4% on an average over the continental areas of the latitude belts containing the Amazonian forest.

[37] From Figures 4a–4c and Table 2, it can be noted that the degradation of the surface due to biomass burning in Amazonia is responsible for the greatest changes in the net infrared radiation and net radiation at the surface, followed by the effect of the smoke aerosol increase. However, the larger amounts of smoke aerosol released in biomass burning in Amazonia seem to play the main role to control

**Table 2.** Changes in the Surface Energy Budgets and in the Evapotranspiration (E), Precipitation (P), and Air Surface Temperature ( $T_a$ ) in the Continental Part of the Latitude Belt Containing the Amazonian Forest (an Average Over This Area) in the Five Experiments<sup>a</sup>

Experiment	Solar Radiation, %	Net Thermal Infrared Radiation, %	Net Radiation, %	H, %	LE, %	E, cm yr <sup>-1</sup>	P, cm yr <sup>-1</sup>	$T_a$ , °C
Degradation of the surface	-6.3	-14.1	-17.5	-14.2	-18.4	-25.3	-26.7	2.0
Smoke aerosols	-9.7	2.2	-14.1	-26.5	-10.5	-13.9	-9.4	0.7
CO <sub>2</sub>	-0.03	0.07	-0.01	-0.06	0.01	0.02	0.16	-0.2
CH <sub>4</sub>	<-0.01	0.01	<-0.01	0.	0.	<0.01	0.02	-0.2
All the changes	-15.3	-9.4	-29.0	-38.6	-26.2	-35.8	-31.8	2.1

<sup>a</sup>Evapotranspiration (E) is given in cm yr<sup>-1</sup>, precipitation (P) is given in cm yr<sup>-1</sup> and air surface temperature ( $T_a$ ) is given in °C. The percentual of the changes in the surface energy budgets are relative to the mean annual values.

the changes in the absorbed solar radiation at the surface. Also, in the latitude belt centered at 5°S, where most of the Amazonian forest is concentrated, the change due to the surface degradation is close to that due to smoke aerosol.

[38] Biomass burning also affects the partition of the available net energy at the surface into sensible and latent fluxes. As can be seen in Figures 5a–5b and Table 2, there is a decrease in both latent and sensible heat fluxes due mainly to the effects of the degradation of the surface and smoke aerosols, while the changes due to CO<sub>2</sub> and CH<sub>4</sub> are too small. The degradation of the surface seems to be the main factor responsible for the reduction of the latent heat flux. On the other hand, the largest changes in the sensible heat flux seem to be due mainly to the release of smoke aerosols in the atmosphere. Reduction in the evapotranspiration leads to a decrease in the latent heat flux in both

cases of degradation of the surface and smoke aerosols. This effect is higher in the case of the degradation of the surface (Figure 5c). Since the surface temperature increases in the two cases (Figure 6) the sensible heat flux would increase. However, a decrease in the sensible heat flux is noted. The reasons are different for the cases of degradation of the surface and smoke aerosols. When the tropical forest is replaced by semi-desert the drag coefficient is greatly reduced and consequently a decrease in the sensible heat flux occurs. Smoke aerosols cause a warming of the earth-atmosphere system. This leads to a smaller difference between the temperatures at the surface and the middle atmosphere and consequently to a reduction in the sensible heat flux compared to the control case. In both the cases the effects of the reduction of the sensible heat flux seem to overcome the effect of the increase of the sensible heat due

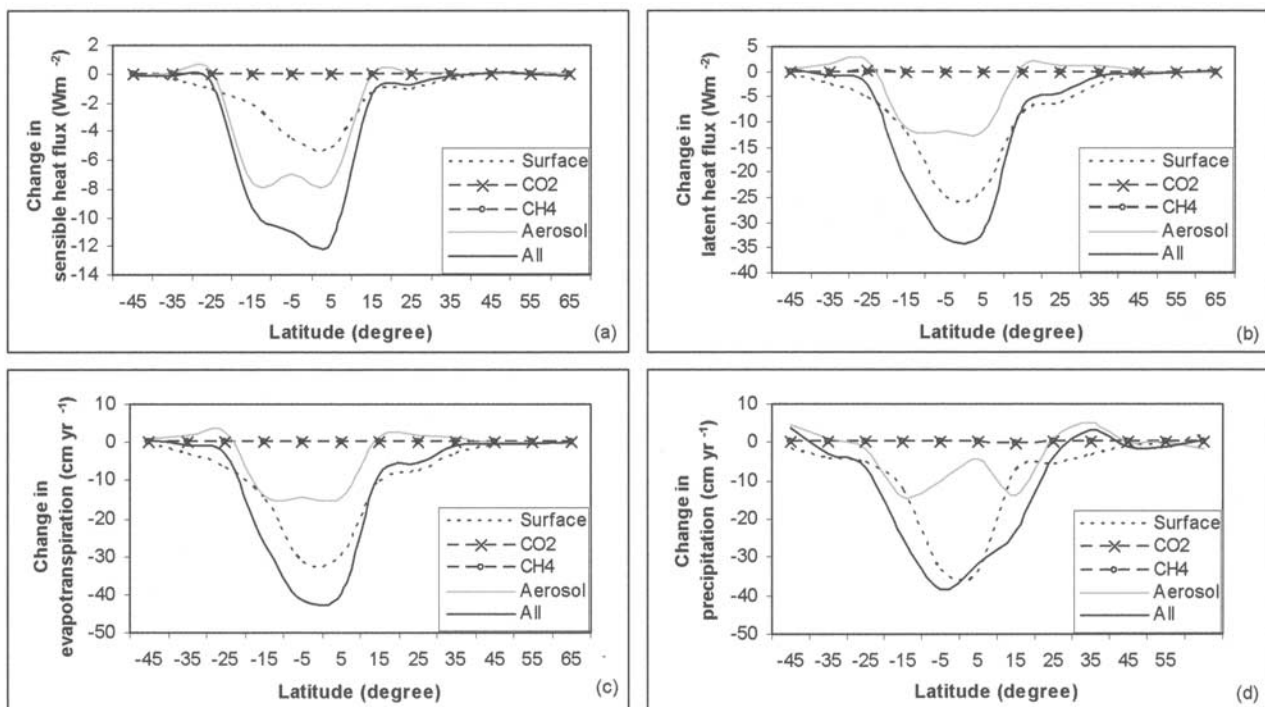


**Figure 5.** Changes in (a) sensible heat flux ( $W m^{-2}$ ), (b) latent heat flux ( $W m^{-2}$ ), (c) evapotranspiration ( $cm yr^{-1}$ ), and (d) precipitation ( $cm yr^{-1}$ ). Legend similar as Figure 4.

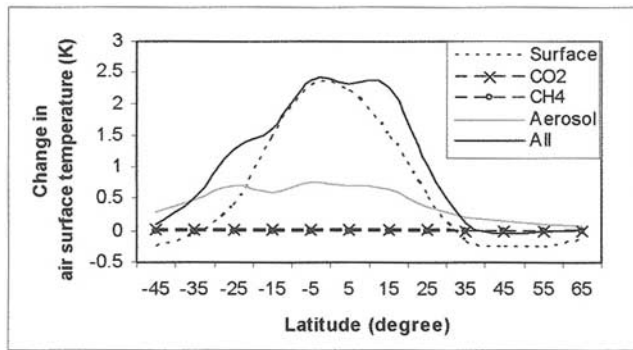


**Figure 6.** Changes in the air surface temperature. Legend similar as Figure 4. Units, °C.

to the surface temperature increase. Since the increase of the surface temperature is higher in the case of the degradation of the surface compared to the smoke aerosols case (Figure 6) the decrease of the sensible heat is lower, as seen in Figure 5a.

[39] From Figures 5a–5b and Table 2 it can be seen that although the changes in the latent heat flux are greater than those in the sensible heat flux, the percentual changes relative to the mean annual conditions are greater in the case of the sensible heat flux. On an average over the continental part of the latitude belts from 20°S to 10°N the sensible and latent heat fluxes decrease by 38.6% and 26.2%, respectively. The reduction in the latent heat flux is due mainly to the effect of the degradation of the surface (18.4%) while the decrease in the sensible heat flux is due mainly to smoke aerosols (26.5%).

[40] As can be seen in Table 2, biomass burning in the Amazonian forest reduces the evapotranspiration and precipitation by 35.8 cm yr<sup>-1</sup> and 31.8 cm yr<sup>-1</sup>, respectively. The greater changes occur at the latitude belt centered at 5°S, which contains the most of the Amazonian forest (reduction of 41.3 cm yr<sup>-1</sup> and 38.5 cm yr<sup>-1</sup> in the evapotranspiration and precipitation, respectively), as shown in Figures 5c–5d. The changes in evapotranspiration and precipitation are due mainly to the degradation of the surface followed by the effect of smoke aerosols. Degradation of the surface is responsible for a reduction of 25.3 cm yr<sup>-1</sup> and 26.7 cm yr<sup>-1</sup> in evapotranspiration and precipitation, respectively, while the decrease due to smoke aerosols corresponds to 13.9 cm yr<sup>-1</sup> and 9.4 cm yr<sup>-1</sup>. Again, the changes due to the greenhouse gases are small, although a slight increase in evaporation and precipitation occurs. Degradation of the surface is also responsible for the largest increase in the air surface temperature (2°C) followed by the smoke aerosols released in the atmosphere (0.7°C), while the greenhouse gases cause a slight reduction in the temperature (0.2°C). When all the effects are considered an increase of 2.1°C occurs, the largest changes (2.4°C) being at the latitude belt centered at 5°S (Figure 6). These results show that the effect of the changes in evapotranspiration is to control the changes in air surface temperature.

[41] The results shown above indicated the relative importance of the changes and mechanisms involved during biomass burning in Amazonian forest. Since all the effects occur simultaneously during fire events a detailed compar-

ison with observed data is a difficult task. Also, the available data correspond to short periods of study and not to mean annual values. Thus mechanistic climate models are a useful tool for investigating separately each effect. Despite the difficulties in comparing with available data, the sign of changes due to smoke aerosols in the present work are in agreement with both observational and radiation model studies. In the experiments regarding the smoke aerosols and greenhouse gases the changes were taken into account using observed values of them. In the case of the degradation of the surface some assumptions were made. After biomass burning occurred in Amazonian forest there is a modification of land surface where large areas of bare soil and trunks lying down the surface are present. Thus land surface parameters such as the surface albedo and roughness length are drastically modified. In the present study, the degradation of the surface due to biomass burning was simulated assuming that the predominant vegetation was modified to semi-desert conditions, except that the soil spectral reflectance was the same as that of the dominant soil in the Amazonian region. Despite the limitations due to assumptions the results showed that the changes due to the degradation of the surface are similar to those obtained from deforestation experiments performed with GCMs.

## 5. Summary and Conclusions

[42] In this paper the effects of biomass burning in Amazonia on climate were studied. Biomass burning produces large amounts of greenhouse gases and aerosols, and modifies the land surface characteristics and, consequently, affects the climate. In order to investigate the relative importance of these changes and the mechanisms involved, a coupled biosphere-atmosphere SDM was used. This kind of model is directed toward understanding the dependence of a particular mechanism on the other parameters of the problem. Since the greenhouse gases and aerosols released in the atmosphere modify the earth's radiation budget, a detailed parameterization of solar radiation and thermal infrared radiation fluxes [Chou and Suarez, 1994, 1999] was included in the SDM.

[43] In the control experiment the mean annual zonally averaged radiation quantities and climate variables were well simulated by the SDM. The simulation of the latitudinal variation of the radiative fluxes matched well the observations. The mean annual global values of radiative quantities simulated by the model were in a good agreement with both observed data and GCM simulations. The climate variables such as air surface temperature, temperature at 500 hPa, 250 hPa zonal wind, vertical velocity at 500 hPa and precipitation were in a good agreement with the NCAR/NCEP reanalysis data sets.

[44] The climatic change due to biomass burning in the Amazonian forest was studied taking into account separately the effects of the degradation of the surface and the changes of the greenhouse gases and aerosols concentrations. In the experiment of the degradation of the surface the evergreen broadleaf trees were replaced by semi-desert in South America from 20°S to 10°N. However, the soil spectral reflectance was the same as that of the dominant soil in the Amazonian region. For investigating the effect of the

changes in the greenhouse gases concentration the SDM was run using typical values of CO<sub>2</sub> and CH<sub>4</sub> concentration noted after burning in a tropical forest. In the experiment of the climate impact of changes in the aerosols concentration AERONET data for a typical region of tropical rain forest with high anthropogenic influence were used. Another experiment considering the effect of all the changes together was made.

[45] The results showed that biomass burning in Amazonia strongly affects the radiative balance at the surface. On an average over the continental portion of the latitude belt containing the Amazonian forest there was a reduction of 15.3% (relative to the annual mean) in the absorbed solar radiation flux at the surface and an increase of 9.4% in the net thermal infrared radiation flux, and consequently the net radiation flux decreased by 29%. The degradation of the surface was responsible for the greatest changes in the net thermal infrared radiation (−14.1%) and net radiation (−17.5%) fluxes at the surface while smoke aerosols seemed to play the main role in controlling the changes in the absorbed solar radiation at the surface (−9.7%). The effects of the degradation of the surface due to biomass burning in Amazonian forest were similar to those obtained in most of deforestation experiments using GCMs: the absorbed solar radiation flux at the surface decreased due to the higher land surface albedo, higher surface temperature lead to an increase of the net thermal infrared radiation, and consequently the net radiation at the surface decreased. To our knowledge, for the first time in this study the effects of the degradation of the surface and smoke aerosols due to biomass burning in Amazonia were investigated together. The effect of the smoke aerosols was to reduce the absorbed solar radiation and the net thermal infrared radiation flux at the surface due to both the higher planetary albedo and atmospheric opacity to longwave radiation. Since there was a decrease in the net radiation at the surface the first mechanism seemed to be more important than the latter.

[46] Biomass burning in Amazonian forest caused decreases of 26.2% and 38.6% in the latent and sensible heat fluxes, respectively. Mainly the degradation of the surface was responsible for the changes in the latent heat flux while smoke aerosol seemed to play a major role in the changes in the sensible heat flux. Latent heat flux decreased due to a reduction in the evapotranspiration. This effect was greater in the case of the degradation of the surface (25.3%) compared to the smoke aerosol case (13.9%). The decrease in evapotranspiration lead to an increase of the air surface temperature of 2°C and 0.7°C in the cases of the degradation of the surface and smoke aerosols, respectively. When the tropical forest was replaced by semi-desert the drag coefficient was greatly reduced. This effect was responsible for decreasing the sensible heat flux in the degradation experiment. Large amounts of smoke aerosols released in the atmosphere caused a warming of the earth-atmosphere system so that the temperature gradient between the surface and middle atmosphere was reduced and consequently there was a decrease in the sensible heat flux. The reduction of the evapotranspiration lead to a decrease in the precipitation (31.8 cm yr<sup>−1</sup>). The greater changes were due to the degradation of the surface (26.7 cm yr<sup>−1</sup>) followed by the release of smoke aerosols (9.4 cm yr<sup>−1</sup>). The changes in the surface energy budget due to the greenhouse gases were

small. This may be attributed to the fact that when biomass burning is occurring in Amazonian forest larger amounts of smoke aerosols are released in the atmosphere compared to the greenhouse gases.

[47] The results showed that in general the greater changes in the radiative balance and climate due to biomass burning in Amazonian forest are caused mainly by the changes in the land surface characteristics, followed by the large amounts of smoke aerosols released in the atmosphere. However, the release of smoke aerosols seems to play the major role in the case of the changes in the solar radiation flux absorbed at the surface and sensible heat flux. Although the changes occur simultaneously and consequently the validation of the model simulations using observed data are a difficult task, the results of each experiment are in general agreement with available observed data and modeling studies.

[48] **Acknowledgments.** We are grateful to Ming-Dah Chou from the Goddard Space Flight Center, NASA, for providing the radiation models code. Thanks are due to Tatiana A. Tarasova for the helpful discussions and to the two anonymous referees for their useful suggestions. This paper forms part of the Ph.D. thesis of the first author.

## References

- Alvalá, P. C., V. W. J. H. Kirchhoff, F. B. Zamorano, and S. C. Casiccia (1996), Atmospheric methane observations in Brazil, SCAR-B Mission, in *SCAR-B Proceedings: Collection of Paper Presented at the Fortaleza, CE, Brazil, Workshop*, edited by V. W. J. H. Kirchhoff, pp. 16–20, Transtec Editorial, São José dos Campos, Brazil.
- Babbitt, R. E., D. E. Ward, R. A. Susott, P. Artaxo, and J. B. Kauffman (1996), A comparison of concurrent airborne and ground-based emissions generated from biomass burning in the Amazon Basin, in *SCAR-B Proceedings: Collection of Paper Presented at the Fortaleza, CE, Brazil, Workshop*, edited by V. W. J. H. Kirchhoff, Transtec Editorial, São José dos Campos, Brazil.
- Barkstrom, B. R., E. Harrison, G. Smith, R. Green, J. Kibler, R. Cess, and the ERBE Science Team (1989), Earth Radiation Budget Experiment (ERBE) archival and April 1985 results, *Bull. Am. Meteorol. Soc.*, 70, 1254–1262.
- Campbell, G. C., and T. H. Vonder Haar (1980), *Climatology of Radiation Budget Measurements From Satellite*, Atmos. Sci. Pap. 323, 74 pp., Dept. Atmos. Sci., Colorado State Univ., Fort Collins, Colo.
- Chou, M.-D. (1984), Broadband water vapor transmission functions for atmospheric IR flux computations, *J. Atmos. Sci.*, 41, 1775–1778.
- Chou, M.-D., and L. Kouvaris (1986), Monochromatic calculations of atmospheric radiative transfer due to molecular line absorption, *J. Geophys. Res.*, 91, 4047–4055.
- Chou, M.-D., and L. Peng (1983), A parametrization of the absorption in the 15 μm CO<sub>2</sub> spectral region with application to climate sensitivity studies, *J. Atmos. Sci.*, 40, 2183–2192.
- Chou, M.-D., and M. J. Suarez (1994), An efficient thermal infrared radiation parameterization for use in general circulation models, Technical Report Series on Global Modeling and Data Assimilation, *Tech. Memo. 104606*, 102 pp., Goddard Space Flight Cent., Greenbelt, Md.
- Chou, M.-D., and M. J. Suarez (1999), A solar radiation parameterization (CLIRAD-SW) developed at Goddard Climate and Radiation Branch for Atmospheric Studies, *NASA Tech. Mem. NASA/TM-1999-104606*.
- Christopher, S. A., M. Wang, T. A. Berendes, and R. M. Welch (1998), The 1985 biomass burning season in South America: Satellite remote sensing of fires, smoke, and regional radiative energy budget, *J. Appl. Meteorol.*, 37, 661–678.
- Crutzen, P. J., L. E. Herdt, J. P. Kransec, W. H. Pollack, and W. Seiler (1979), Biomass burning as a source of atmospheric gases CO, H<sub>2</sub>, N<sub>2</sub>, CH<sub>3</sub>Cl, and CO<sub>2</sub>, *Nature*, 282, 253–256.
- Dickinson, R. E., and P. J. Kennedy (1992), Impacts on regional climate of Amazonian deforestation, *Geophys. Res. Lett.*, 19, 1947–1950.
- Dickinson, R. E., A. Henderson-Sellers, P. J. Kennedy, and M. F. Wilson (1986), *Biosphere-Atmosphere Transfer Scheme (BATS) for the NCAR Community Climate Model*, NCAR Tech. Note 275+STR.
- Ellis, J. S., and T. H. Vonder Haar (1976), *Zonal Average Earth Radiation Budget Measurements From Satellite for Climate Studies*, Performing Org. Rep. No. 240, 63 pp., Dept. Atmos. Sci., Colorado State Univ., Fort Collins, Colo.

- Franchito, S. H., V. B. Rao, and R. R. Silva (1998), A parameterization of radiative fluxes suitable for use in a statistical-dynamical model, *Meteorol. Atmos. Phys.*, *69*, 23–38.
- Fu, Q., and K. N. Liou (1992), On the correlated k-distribution method for radiative transfer in nonhomogeneous atmosphere, *J. Atmos. Sci.*, *49*, 2139–2156.
- Hahn, C. J., W. B. Rossow, and S. G. Warren (2001), ISCCP Cloud properties associated with standard cloud types identified in individual surface observation, *J. Clim.*, *14*, 11–28.
- Holben, B. N., et al. (2001), An emerging ground-based aerosol climatology: Aerosol optical depth from AERONET, *J. Geophys. Res.*, *106*, 12,067–12,097.
- Houghton, J. T., Y. Ding, D. J. Griggs, M. Noguer, P. J. van der Linden, X. Dai, K. Maskell, and C. A. Johnson (Eds.) (2001), *Climate Changes 2001: The Scientific Basis: Contribution of Working Group I to the Third Assessment Report of the Intergovernmental Panel on Climate Change*, 881 pp., Cambridge Univ. Press, New York.
- Lean, J., and P. R. Rowntree (1993), A GCM simulation of the impact of Amazonian deforestation on climate using an improved canopy representation, *J. R. Meteorol. Soc.*, *119*, 509–530.
- Lean, J., and P. R. Rowntree (1997), Understanding the sensitivity of a GCM simulation of Amazonian deforestation to the specification of vegetation and soil characteristics, *J. Clim.*, *10*, 1216–1235.
- Li, Z. Q., and H. G. Leighon (1993), Global climatologies of solar radiation budgets at the surface and in the atmosphere from 5 years of ERBE data, *J. Geophys. Res.*, *98*, 4919–4939.
- McClatchey, R. A., R. W. Fenn, J. E. A. Selby, F. E. Voltz, and J. S. Garing (1972), Optical properties of the atmosphere, *Tech. Rep. AFCRL-72-0497*, 108 pp., Air Force Cambridge Res. Lab., Bedford, Mass.
- Mobley, C. D. (1994), *Light and Water: Radiative Transfer in Natural Waters*, 592 pp., Academic, San Diego, Calif.
- Nobre, C. A., P. J. Sellers, and J. Shukla (1991), Amazonian deforestation and regional climate change, *J. Clim.*, *4*, 957–988.
- Nobre, C. A., L. F. Mattos, C. P. Dereczynski, T. A. Tarasova, and I. V. Trosnikov (1998), Overview of atmospheric conditions during the smoke, cloud, and Radiation-Brazil (SCAR-B) field experiment, *J. Geophys. Res.*, *103*, 31,809–31,820.
- Ohmura, A., H. Gilgen, and Global Energy Balance Archive (GEBA) (1991), World Climate Program-Water Project A7, *Rep. 2*, The Geba Database Interactive Application, Retrieving Data, 60 pp., Int. Council of Sci. Unions, World Meteorol. Org., Zurich.
- Ou, S. C. S., K. N. Liou, and W. J. Liou (1989), The seasonal cycle of the global zonally averaged energy balance, *Theor. and Appl. Climatol.*, *40*, 9–23.
- Peixoto, J. P., and A. H. Oort (1992), *Physics of Climate*, 520 pp., Am. Inst. of Phys., New York.
- Tarasova, T. A., C. A. Nobre, B. N. Holben, T. F. Eck, and A. W. Setzer (1999), Assessment of smoke aerosol impact on surface solar irradiance measured in the Rondonia region of Brazil during smoke, cloud, and radiation- Brazil, *J. Geophys. Res.*, *104*, 19,161–19,170.
- Tarasova, T. A., C. A. Nobre, B. N. Holben, T. F. Eck, and A. Setzer (2000), Modeling of gaseous, aerosol, and cloudiness effects on surface solar irradiance measured in Brazil's Amazonia 1992–1995, *J. Geophys. Res.*, *105*, 26,961–26,969.
- Varejão-Silva, M. A., S. H. Franchito, and V. B. Rao (1998), A coupled biosphere-atmosphere climate model suitable for use in climatic studies due to land surface alterations, *J. Clim.*, *11*, 1749–1767.
- Wilber, A. C., D. P. Kratz, and S. K. Gupta (1999), Surface emissivity maps for use in satellite retrieval of longwave radiation, *NASA/TP-1999-209362*, 35 pp., NASA, Washington, D. C.
- Wild, M., H. Ohmura, E. Gilgen, E. Roeckner, M. Giorgetta, and J. J. Morcrette (1998), The disposition of radiative energy in the global climate system: GCM-calculated versus observational estimates, *Clim. Dyn.*, *14*, 853–869.
- World Meteorological Organization (1986), A preliminary cloudless standard atmosphere for radiation computation, *Rep. WCP-112, WMO/TD-No. 24*, 53 pp., World Clim. Res. Prog., Geneva.
- Zhang, T. (1994), Sensitivity properties of a biosphere model based on BATS and a statistical-dynamical climate model, *J. Clim.*, *7*, 891–913.

---

V. Brahmananda Rao and S. H. Franchito, Centro de Previsão de Tempo e Estudos Climáticos (CPTEC), Instituto Nacional de Pesquisas Espaciais (INPE), CP 515, 12201-970, São José dos Campos, SP, Brazil.

E. C. Moraes, Divisão de Sensoriamento Remoto (DSR), Instituto Nacional de Pesquisas Espaciais (INPE), CP 515, 12201-970, São José dos Campos, SP, Brazil. (bete@dsr.inpe.br)